Langmuir

Letter

pubs.acs.org/Langmuir

How Surface Functional Groups Influence Fracturation in Nanofluid Droplet Dry-Outs

Florian Carle* and David Brutin*

Aix-Marseille University, IUSTI UMR 7343 CNRS, 13013 Marseille, France

Supporting Information

ABSTRACT: In this study of drying water-based nanofluid droplets, we report the influence of surface functional groups and substrate surface energies on crack formation and dry-out shape. These two key parameters are investigated by allowing nanofluids with several functional groups grafted on polystyrene nanoparticle surfaces to dry on various substrates. These experiments result in a variety of regular crack patterns with identical nanoparticle diameter, material, concentration, and drying conditions. We demonstrate that, despite the various patterns observed, the crack spacing/deposit height ratio is constant for similar substrate surface energies and linearly increases with this parameter. Moreover, this study shows that the crack shape is strongly influenced by surface functional groups as a result of particle interactions (depending on the particle surface potentials) and compaction during solvent evaporation.

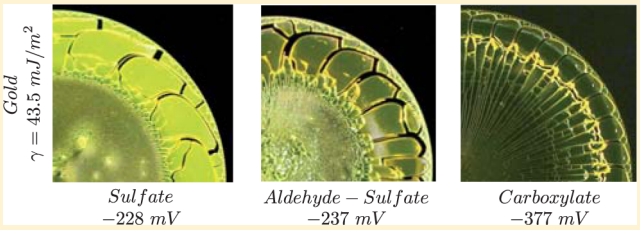

INTRODUCTION

The most commonly used coating process by far is the deposition of particles onto the desired medium via solvent evaporation. The recent heavy use of nanofluids over the past decade is a good indication that nanofluids will soon be widely used by research and industrial communities for coating processes and drying applications. Thin, compact layers of nanoparticles can have useful applications for the modification of surface properties[1] such as wetting, electrical conductivity, and energy storage[2,3] or for improving materials by applying high scratch- and wear-resistant nanoclear coats as used in automobile applications.[4] These applications often require deposits that are free of defaults, such as imperfections, warping, and cracks. However, when fluids containing immiscible particles (from nanofluids to colloid suspensions[5−8] including larger-scale event such as slurries and mud[9]) dry, the deposits tend to crack and even delaminate from the substrate.[10] Crack formation is influenced by a large set of parameters: particle size, concentration,[11−14] shear modulus of the particles,[6] and also evaporation dynamics.[12,15]

Because nanofluids tend to be unstable and to flocculate, surfactants or functional groups are used to form either a steric barrier (e.g., polymers and plasticisers) or an ionic barrier (e.g., electrostatic stabilization from the electric double layer and from sol−gel precursors) to keep the particles separated and to avoid clusters. These additions greatly modify the suspensions but have yet to be investigated for their influence on crack patterns. In this article, we demonstrate that surface functional groups (SFGs) have a strong effect on the final crack patterns of dry-outs of nanofluids. To our knowledge, SFGs have never before been taken into account in studies on drying, crack patterns, and the self-assembly of nanoparticles. These functional groups are, however, widely used in several communities as biological tracers with fluorescent spheres, cancer treatment using their surface functional groups to bond a dedicated protein,[16] and even inkjet printers using metallic nanoparticles to create monatomic layers on various hydrophilic and hydrophobic substrates.[17] For all of these applications, SFGs are crucial for nanoparticles to be compatible with a variety of conjugation strategies. Both nanoparticle convective self-assembly and the final crack patterns are affected by physicochemical interactions with SFGs. Interactions between SFGs[18] and solvents[19] were investigated, but more research is needed on the influence of the interaction between SFGs during the formation of close-packed particle assemblies and also on fracturing during drying.

MATERIALS AND METHODS

Nanofluid Properties. To have a better understanding of this matter, three SFGs were investigated (carboxylate, −COOH; sulfate $-HSO_4$; and aldehyde sulfate, $-CH_2O$). Briefly, the experiment consisted of gently laying down droplets of nanofluids onto three different substrates (glass, poly-L-lysine, and gold) and then allowing the droplets to evaporate freely inside a humidity-regulated (50 ± 1%) glovebox at atmospheric pressure to avoid external perturbation during drying. Droplets were created using an electronic syringe to ensure a constant droplet volume of 4 μL for all experiments. Mass transfer of water from the drop to ambient air is limited by diffusion (because of the presence of surrounding convection in the vapor phase) and is controlled by relative humidity, which was kept constant. All droplets reported here are water-based 2 ± 0.03% by mass bright-yellow polystyrene nanoparticles with a density that is almost the same as that of the solvent (density is 1.05). Three different SFGs were used to change the chemical potential of the particles to make them more hydrophilic and less likely to bind to negatively charged elements.

Received: April 17, 2013
Revised: July 26, 2013
Published: July 26, 2013

Table 1. (Top) Nanofluid Chemical and Physical Properties at 25°C and 1 atm[a] and (Bottom) Substrates Chemical and Physical Properties[b]

SFG	*D*nm	*C*(no./mL)	*q*(meq/g)	ψ_0(mV)	SSA m^2/g	SSA m^2/mL	pH
sulfate	22	3.4×10^{15}	0.0599	−228	260	5.17	5.14
carboxylate	24	2.6×10^{15}	0.7152	−377	240	4.74	7.47
aldehyde-sulfate	24	2.6×10^{15}	0.0658	−237	240	4.74	5.37

substrate	rrms (nm)	γ_P (mJ/m^2) (%)	γ_D (mJ/m^2) (%)	γ_T (mJ/m^2) (%)
glass	25	31.0 ± 0.4	40.4 ± 0.4	71.4 ± 0.4
poly-L-lysine	10	22.1 ± 0.4	43.4 ± 0.2	65.5 ± 0.3
gold	4	2.8 ± 7.4	40.7 ± 2.7	43.5 ± 3.0

[a]All three nanofluids are 2% by mass in concentration. In the table, *D* is the particle diameter (uncertainty of the nanoparticle diameter is ±0.3 nm), *C* is the particle concentration, *q* is the charge, and SSA is the specific surface area. The last column gives the pH (uncertainty about ±0.05 and the solvent (water) pH 7.94.). [b]25 mm × 75 mm × 1 mm slides.

Carboxylate nanoparticles were obtained by grafting polymers containing pendant carboxylic acid groups to sulfate nanopsheres, whereas aldehyde sulfate was modified by the addition of surface aldehyde groups. These nanofluids were selected for their stability (several months because of the presence of a small quantity of sodium azide), size homogeneity (diameter $D \pm 3$ nm), and surface potential ψ_0 (Table 1). The nanofluid charge *q* has been measured by titation by the manufacturer and allows access to ψ_0 via eq 1 (see below).

Substrate Physical Properties. By coupling these different SFGs with substrates having different surface energies, we demonstrate the effect of this coupling on the deposition pattern both locally and globally. Any differences in cracks, delamination, or the deposition of matter will be due to only these coupling mechanisms. The substrates were chosen because of their particular surface free energies (from low to high surface energy: glass, glass coated with poly-L-lysine, and silicone coated with gold) and because they possess fairly small roughness (smooth substrates), which was characterized using confocal microscopy. The substrate properties are summarized in Table 1. The purpose of this study is not to change the surface topology but only the physiochemical interactions in between the substrate charges and the nanofluid SFGs. The substrate surface energies have been measured with the Owens−Wendt method, which is based on the Young equation (links the droplet contact angle with the substrate surface energy) and Good's equation (links the droplet interface tension with the dispersive and polar components of the surface energy). The uncertainty of the value is due to the difficulty of measuring droplet contact angles and the Berthelot hypothesis, which equalizes the interaction between molecules of the fluid and substrate layers with the geometric intermolecular interaction of each substance (fluid or substrate).[20] The substrates have similar dispersive surface energy components γ_D (about 40 mJ/m^2), but the polar component γ_P varies from 2.8 to 31 mJ/m^2, resulting in good wetting of the nanofluid on glass (average initial contact angle $\theta_i = 11°$), intermediate wetting on lysine ($\theta_i = 31°$), and quasihydrophobic on gold ($\theta_i = 65°$). Extra-clean gold substrates are known to be widely hydrophilic (with a contact angle near 0°); our substrates were kept in a clean environment but in contact with air to enable carbonaceous contamination of the surface, resulting in a transition from a hydrophilic to a hydrophobic wetting situation.[21] Advancing and receding contact angles were measured for each configuration (fluids and substrates, data available in the Supporting Information) and displayed important hysteresis (up to 50° for a gold substrate) because of particle deposition onto the substrate, pinning the contact line. The nanoparticles not only modify the roughness locally but also change the solid/liquid interfacial tension, leading to important hysteresis.

Evaporation Dynamics and Deposition Profiles. During solvent evaporation and droplet drying, image analysis was performed using a digital camera to visualize the drop from above (Figure 1), which gave a good representation of droplet evolution in enough detail for additional analysis of specific areas. As soon as the fluid touches the substrate, the droplet spreads to reach its maximum wetting diameter. The contact line is pinned during most of the evaporation process, whereas the contact angle and the height decrease linearly. After a few minutes (Figure 1, image 2), a circular deposit is clearly visible at the edge of the drops as a result of the capillary flow generated to compensate for the evaporation loss at the contact line.[22] Because the evaporation dynamics of a droplet are closely linked to the geometric behavior along the contact line, the evaporation flux rate of the droplet on glass is higher than that on lysine and even higher than that on gold. Therefore, the particles are dragged outward with this flow in a fairly rapid process and then form deposits. As the solvent evaporates, the particles are forced to concentrate in a close-packed array. For the particle depositions at the rim where the contact line is pinned to the substrate, the fluid/solid binary plays an important role in the width and height of the coronas, as can be seen in Figure 2, upper graph. Interestingly, the coronas not only differed in height but also differed in width as the substrate surface energies decreased. The heights and radii were normalized (Figure 2, graphs on the right) to allow for a comparison of the droplet coronas. The deposit heights were measured using confocal microscopy. Because droplets dry on perfectly horizontal surfaces and the evaporation dynamics is similar on each point of the triple line, deposits formed on the substrate are axisymmetric (the average eccentricity of the droplets is about 0.12), except for isolated defaults such as dust or irregular cracks. To reduce their impacts, the height profiles shown in both graphs were obtained using SPIP (a software package for nano- and microscale image processing) by the average of the radii height profiles for at least 180 radii of the deposit. The average standard deviation at the highest points is about 1.0 μm. Because the deposits present cracks, the averaging process underestimates the deposit height. Figure 2 give a good estimation of radius r_0 of the deposit's highest point. (See the example of the aldehyde sulfate deposit on lysine.)

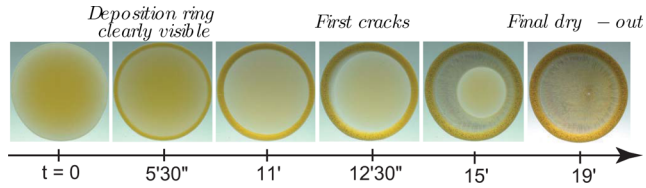

Figure 1. Evaporation of a 4 μL aldehyde sulfate nanofluid droplet onto a lysine substrate at 24 °C and 50% humidity (movie in Supporting Information).

The pinned evaporation continues for about 60% of the total time of evaporation until the contact line recedes when the critical contact angle is exceeded. The depinned contact line shrinks toward the center (Figure 1, picture 3). The motion of the solvent induces a stress in all deposits, and cracks start to nucleate (picture 4). Once all the solvent is evaporated, the dried particles completely cover the initial wetting area because of their relatively high concentration and form regular crack patterns (Figure 3). Experiments were performed several times for each configuration, and the crack patterns are reproducible.

Figure 3, if observed vertically, shows the final crack patterns of each nanofluid on the three substrates (surfaces are characterized by their

dx.doi.org/10.1021/la401428v | Langmuir 2013, 29, 9962−9966

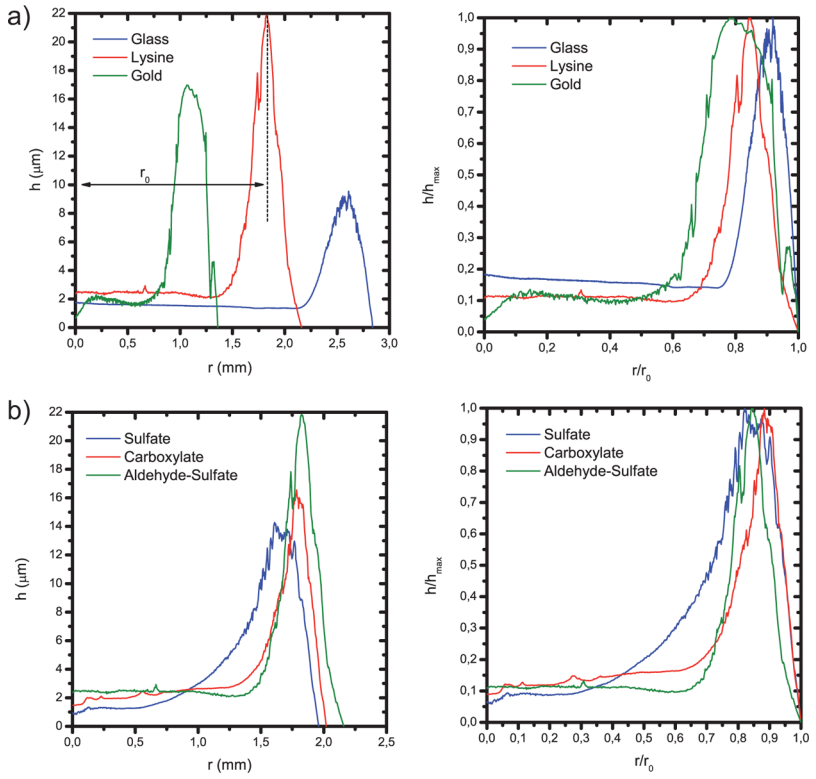

Figure 2. Deposit height profiles (left) and normalized deposit height profiles (right) of (a) aldehyde sulfate nanofluid droplets on the three substrates and (b) three nanofluid droplets on lysine substrates.

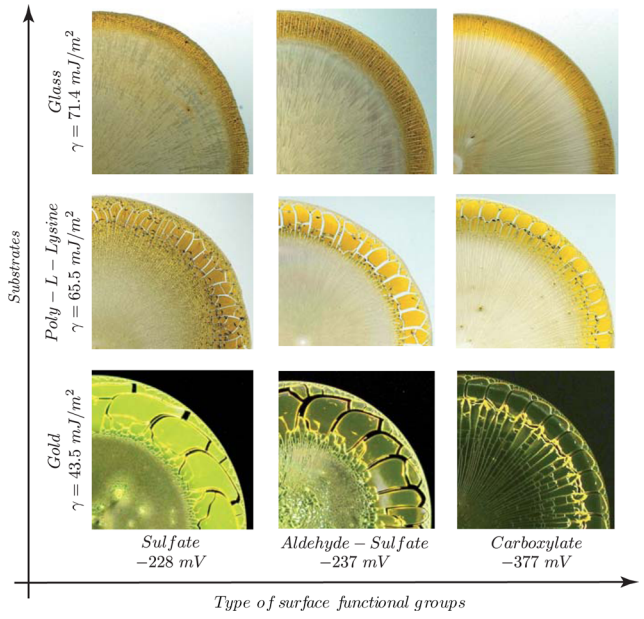

Figure 3. Dry-out characteristics for the binary fluid/solid configurations and final crack pattern after evaporation at 24 °C and 50% humidity for a colloidal suspension of 24-nm-diameter polystyrene nanoparticles coated with three different surface functional groups (SFGs) having different surface free energies.

increasing surface energy) and if observed horizontally shows the effect of SFGs on cracks (characterized by their increased electrical charge in solution in meq/g).

Crack Formation. Two different sets of cracks are visible on the droplet dry-outs: large radial cracks and smaller orthoradial ones with a much shorter characteristic length. In such an isotropic material, cracks tend to form and grow in the direction in which the release of strain energy is the maximum.[7] In this configuration, the stress in the deposit is due to capillary forces that develop as the solvent evaporates.

In the early stages of evaporation, particles are free to move in the solvent by Brownian motion, and the separation between them is subjected to DLVO theory, where van der Walls forces are balanced by ionic repulsive forces. As the solvent evaporates, the average distance between particles must be reduced to keep all of them inside the fluid; if a particle get exposed to air at the edge of the drop contact line, then the surface energy will increase locally[23] and will change the force balance. Particle reorganization in the external layer of the deposit can accommodate some of the strain, but the particles inside the lower layer tend to bind to the substrate and tend to resist deformation, thereby preventing any possible relaxation.[24] This phenomenon leads to an increase in stress, which is subsequently relaxed by plastic deformation and crack nucleation.

Large cracks are the first to form and do so in the direction of evaporation to release the stress induced by solvent evaporation and by particle adhesion to the substrate. The stress in a gel had previously been quantified for a confined system,[25] but for droplets, however, an experimental determination of the stress in such an open configuration is almost impossible; numerical analysis should instead be used. The opening of the material allows the remaining solvent, hitherto confined under the deposit, to evaporate; drainage increases the stress in large plates of particles. The stress gets released with the formation of smaller orthoradial cracks between the large cracks. Because of the axisymmetrical aspect of the system, the stress generated by evaporation is identical at each point in the drop. In the vicinity of a crack, the stress is null and increases with distance from the crack. When the stress reaches a maximum and exceeds the fracture strength, a new crack nucleates. The same phenomenon happens in the deposit in the vicinity of this new crack, which forms another crack, thus inducing crack formation with a regular periodicity λ_0 (Figure 2). This periodicity has been measured at the highest point of the corona (Figure 2) in the direction of the circumference. The perimeter is divided by the number of cracks manually obtained on magnified pictures of the final pattern to access the average crack spacing λ_0; this has been possible thanks to the very high quality level of the pictures taken during the experiments. The

dx.doi.org/10.1021/la401428v | Langmuir 2013, 29, 9962−9966

uncertainty in the number of cracks has been overestimated (±2 cracks for the droplets on gold substrates, ±5 cracks on lysine, and up to ±10 cracks on glass).

Influence of the Fluid/Solid Binary on the Dry-Out Patterns. These crack networks form a general pattern in the dry-outs and are composed of a thick corona on the rim, which contains the majority of the particles, and of central area with many fewer particles. Although the particle concentration is too high to form "coffee stain"-like patterns,[11,22] the height of the corona is greater than that of the central area (Figure 2). The additional height explains the formation of three crack patterns. As previously explained for confined configurations, the stress increases in the material with increasing distance but also increases with increasing thickness of the deposits.[5] Figure 5 confirms this assumption for the droplet configuration and displays the ratio of length wave/deposit height as a function of the initial contact angle. The figure demonstrates that this ratio increases linearly with the contact angle (i.e., with decreasing surface energy). The three clusters of points represent droplets on the three substrates. On glass, the weak deposit and the high surface energy of the substrate induced a short wavelength ($\lambda_0 \approx 11\ \mu$m, Figure 3). In this case, the material must relax stress more frequently. However, on gold, the low adhesion and thick deposit allow the material to resist stress better. Thus, crack formation is not required as often as on glass; gold induces a longer wavelength ($\lambda_0 \approx 72\ \mu$m).

Influence of Surface Potential on Cracks. If we now consider the three nanofluids on the same substrate, because the diameter, wetting situation, evaporation dynamics on their respective substrates, and deposit profiles (Figure 4) are all similar, one might assume that the

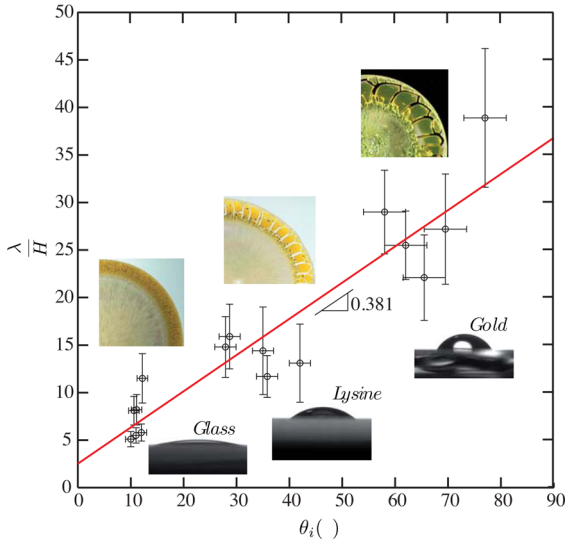

Figure 4. Crack spacing/deposit height ratio plotted as a function of the initial contact angle. Side and top views show the behavior of both aldehyde sulfate droplets on the substrates and the crack patterns formed. Information about the linear fit: $^{\lambda}/_{H} = 0.381\theta_i + 2.522$.

cracks form because of stress, as explained previously, and that they will form similar patterns. However, upon further inspection of Figure 3 in the horizontal direction, the final crack patterns are clearly different, with wavelengths ranging from 301 μm for carboxylate on gold to 442 μm for aldehyde sulfate. Although similar in height (about 14 μm), the deposits are also different. The slopes leading from the corona to the center (Figure 2b) have different gradients. The deposition profile is controlled by the evaporation dynamics; the particle is dragged outward by the fluid motion inside the droplet. Because the evaporation flux rate is similar for a given substrate, the fluid motion is also similar and creates identical coronal outer slopes. At the inner slope of the corona, depinning of the contact line and its recession toward the center drag the particles that convectively self-assembled during the early stages of evaporation. The particles are able to stay in their current positions fairly well depending on their electrical charge.

Each particle in the solvent phase is stabilized by an SFG to repel van der Waals forces and to avoid flocculation. Depending on the type of SFGs, ionic charges (measured by titation, Table 1) change the surface potential ψ_0. This potential has been calculated using the Grahame equation[26]

$$\psi_0 = \frac{2kT}{C} a \sinh\left(\frac{\sigma}{\sqrt{8\varepsilon\varepsilon_0 kT\frac{C}{2}N_a}}\right) \quad (1)$$

where k is Boltzmann's constant, T is temperature, C is the ionic concentration, σ is the surface charge density, ε_0 and ε are the permittivitites of free space and of the material, respectively, and N_A is Avogadro's constant. For carboxylate, the surface potential is −377 mV, which induces good adhesion between particles and makes contact line recession less prone to move particles. However, for sulfate, a zeta potential of −228 mV lets the particles reorganize more easily and induces a deposit profile featuring a corona with a shallower inner slope.

Nanoparticle Compaction. To observe the direct effect of the surface potential, the deposits were observed under a scanning electron microscope (SEM) to visualize the topography and the microstructure of the dry-out (Figure 5). Unlike previous studies, which had found that

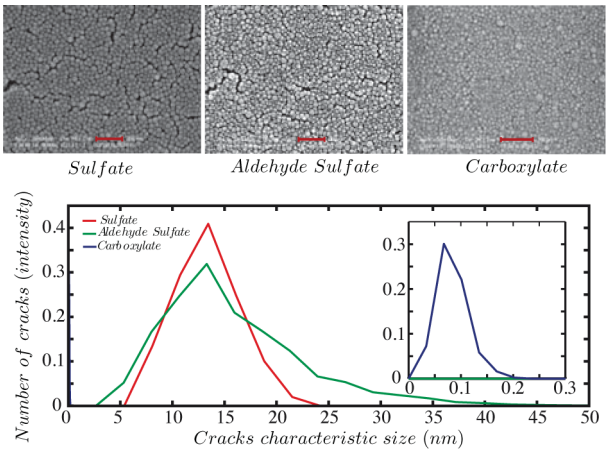

Figure 5. Particle assemblies observed by scanning electron microscopy (scale 200 nm) with their corresponding granulometries. (Inset) Enlarged image.

particles agglomerated into an organized pattern (either square[27] or hexagonal packing[28−30]), these particles exhibited a disordered close-packed configuration. This absence of a characteristic configuration could come from the polydispersity of the particles observed after complete drying. Askounis et al. did not observe any remarkable configurations in drying TiO_2 nanofluids.[31]

The crack spacing was slightly different for the particles grafted with sulfate and aldehyde sulfate (average characteristic crack size approximately 14 nm) and less than 1 nm for the particles grafted with carboxylate (Figure 5).

The hypothesis that the surface potential plays a major role in particle organization was confirmed by the sample granulometry. The close compaction of the particles grafted with carboxylate SFG is due to the high surface potential of the nanofluid. The two other nanofluids with similar surface potentials present a similar compaction, larger than carboxylate particles, as a result of a smaller charge. The difference in particle crack spacing is due to the difference in surface potential.

■ CONCLUSIONS

The role of SFGs in the drying of sessile droplets was experimentally investigated. Three similar nanofluids containing particles grafted with carboxylate, sulfate, and aldehyde sulfate functional groups were deposited on substrates with various surface energies in order to investigate the fluid/solid binary

dx.doi.org/10.1021/la401428v | Langmuir 2013, 29, 9962−9966

influence on crack formation. By changing the substrates, we have demonstrated that the crack wavelength/deposit height ratio increases linearly with the surface energy but stays relatively constant for various functional groups. Moreover, at a constant ratio, droplets present fairly different cracks in shape yet regular formations. This study found that SFGs play a major role in crack patterns (e.g., modification of shape) and in particle compaction (e.g., modification in granulometry). The deposition height profiles on similar substrates are also influenced by the surface functional group during the depinning of the contact line. Despite these drastic effects, SFGs have not been investigated in studies about dry-out cracks and should be investigated carefully in more detail. Future research will investigate the stress on particles induced by evaporation for unconstrained droplets.

■ ASSOCIATED CONTENT

Supporting Information

Movie of a droplet drying, experimental procedures, optical setup specifications, and hysteresis measurements. This material is available free of charge via the Internet at http://pubs.acs.org/.

■ AUTHOR INFORMATION

Corresponding Author

*E-mail: florian.carle@etu.univ-amu.fr; david.brutin@univ-amu.fr.

Notes

The authors declare no competing financial interest.

■ ACKNOWLEDGMENTS

We thank both the Centre National d'Etude Spatiales in the framework of the Droplet Evaporation grant and CARNOT Star in the framework of the NPC grant for financial support. We also acknowledge both Jean-Jacques Simon and Ludovic Escoubas of the IM2NP laboratory for granting the use of the confocal microscope, Jean-Baptiste Lang for performing the preliminary experiments, and Jerome Vicente for advice on the droplet dry-out thickness averaging.

■ REFERENCES

(1) Park, K.; Son, J.; Chung, H.; Kim, S.; Lee, C.; Kang, K.; Kim, H. Surface modification by silver coating for improving electrochemical properties of $LiFePO_4$. *Solid State Commun.* **2004**, *129*, 311−314.

(2) Mpourmpakis, G.; Froudakis, G. E.; Lithoxoos, G. P.; Samios, J. SiC nanotubes: a novel material for hydrogen storage. *Nano Lett.* **2006**, *6*, 1581−1583.

(3) Pumera, M. Graphene-based nanomaterials for energy storage. *Energy Environ. Sci.* **2011**, *4*, 668−674.

(4) Mohseni, M.; Ramezanzadeh, B.; Yari, H.; Moazzami, M. In *New Advances in Vehicular Technology and Automotive Engineering*; Carmo, J., Ed.; InTech: New York, 2012; pp 1−5.

(5) Allain, C.; Limat, L. Regular patterns of cracks formed by directional drying of a collodia suspension. *Phys. Rev. Lett.* **1995**, *74*.

(6) Singh, K. B.; Tirumkudulu, M. S. Cracking in drying colloidal films. *Phys. Rev. Lett.* **2007**, *98*, 218302.

(7) Goehring, L.; Clegg, W. J.; Routh, A. F. Wavy cracks in drying colloidal films. *Soft Matter* **2011**, *7*, 7984.

(8) Goehring, L.; Clegg, W. J.; Routh, A. F. Plasticity and fracture in drying colloidal films. *Phys. Rev. Lett.* **2013**, *110*, 024301.

(9) Goehring, L.; Conroy, R.; Akhter, A.; Clegg, W. J.; Routh, A. F. Evolution of mud-crack patterns during repeated drying cycles. *Soft Matter* **2010**, *6*, 3562−3567.

(10) Pauchard, L. Patterns caused by buckle-driven delamination in desiccated colloidal gels. *Europhy. Lett.* **2006**, *74*, 188−194.

(11) Chon, C. H.; Paik, S.; Tipton, J. B.; Kihm, K. D. Effect of nanoparticle sizes and number densities on the evaporation and dryout characteristics for strongly pinned nanofluid droplets. *Langmuir* **2007**, *23*, 2953−2960.

(12) Brutin, D. Influence of relative humidity and nano-particle concentration on pattern formation and evaporation rate of pinned drying drops of nanofluids. *Colloids Surf., A* **2013**, *429*, 112−120.

(13) Kim, I. T.; Kihm, K. D. Unveiling hidden complex cavities formed during nanocrystalline self assembly. *Langmuir* **2009**, *25*, 1881−1884.

(14) Kim, I. T.; Kihm, K. D. Hidden cavity formations by nanocrystalline self-assembly on various substrates with different hydrophobicities. *Langmuir* **2012**, *28*, 9195−9200.

(15) Deegan, R. Pattern formation in drying drops. *Phys. Rev. E* **2000**, *61*, 475.

(16) Arima, Y.; Iwata, H. Effect of wettability and surface functional groups on protein adsorption and cell adhesion using well-defined mixed self-assembled monolayers. *Biomaterials* **2007**, *28*, 3074−3082.

(17) Chhasatia, V. H.; Sun, Y. Interaction of bi-dispersed particles with contact line in an evaporating colloidal drop. *Soft Matter* **2011**, *7*, 10135.

(18) Frisbie, C. D.; Rozsnyai, L. F.; Noy, A.; Wrighton, M. S.; Lieber, C. M. Functional group imaging by chemical force microscopy. *Science* **1994**, *265*, 2071−2074.

(19) Halicioglu, T.; Jaffe, R. L. Solvent effect on functional groups attached to edges of carbon nanotubes. *Nano Lett.* **2002**, *2*, 573−575.

(20) Rudawska, A.; Jacniacka, E. Analysis for determining surface free energy uncertainty by the Owen/Wendt method. *Int. J. Adhes. Adhes.* **2009**, *29*, 451−457.

(21) Smith, T. The hydrophilic nature of a clean gold surface. *J. Colloid Interface Sci.* **1980**, *75*, 51−55.

(22) Deegan, R. D.; Bakajin, O.; Dupont, T. F.; Huber, G.; Nagel, S. R.; Witten, T. A. Capillary flow as the cause of ring stains from dried liquid drops. *Nature* **1997**, 827−829.

(23) Holmes, D.; Tegeler, F.; Clegg, W. Stresses and strains in colloidal films during lateral drying. *J. Eur. Ceram. Soc.* **2008**, *28*, 1381−1387.

(24) Chiu, R. C.; Garino, T. J.; Cima, M. J. Drying of granular ceramic films: I, effect of processing variables on cracking behavior. *J. Am. Ceram. Soc.* **1993**, *76*, 2257−2264.

(25) Zarzycki, J. Critical stress intensity factors of wet gels. *J. Non-Cryst. Solids* **1988**, *100*, 359−363.

(26) Israelachvili, J. N. *Intermolecular and Surface Forces*, 3rd ed.; Academic Press: Burlington, MA, 2010.

(27) Marin, A.; Gelderblom, H.; Lohse, D.; Snoeijer, J. Order-to-disorder transition in ring-shaped colloidal stains. *Phys. Rev. Lett.* **2011**, *107*.

(28) Prevo, B. G.; Velev, O. D. Controlled, rapid deposition of structured coatings from micro- and nanoparticle suspensions. *Langmuir* **2004**, *20*, 2099−2107.

(29) Goehring, L.; Clegg, W. J.; Routh, A. F. Solidification and ordering during directional drying of a colloidal dispersion. *Langmuir* **2010**, *26*, 9269−9275.

(30) Askounis, A.; Sefiane, K.; Koutsos, V.; Shanahan, M. E. R. Structural transitions in a ring stain created at the contact line of evaporating nanosuspension sessile drops. *Phys. Rev. E* **2013**, *87*, 012301.

(31) Askounis, A.; Orejon, D.; Koutsos, V.; Sefiane, K.; Shanahan, M. E. R. Nanoparticle deposits near the contact line of pinned volatile droplets: size and shape revealed by atomic force microscopy. *Soft Matter* **2011**, *7*, 4152−4155.